Biological Simulation of Scale-invariant Time Cells

Yue Liu, Zoran Tiganj, Michael E. Hasselmo, Marc W. Howard
Boston University

Abstract

Scale-invariant timing has been observed in a wide range of behavioral experiments. The scale-invariant firing property of recently described *time cells* provides a possible neural substrate for this behavior. Earlier work proposed a mathematical model that generates scale-invariant time cells based on neurons with long time constants and an approximation of inverse Laplace transform. This paper presents a biologically detailed network model of this mathematical algorithm. The simulations incorporate exponentially decaying persistent firing maintained by the CAN-current and a network structure given by the inverse Laplace transform to generate time cells with scale-invariant firing rates. This model provides the first biologically detailed neural circuit for generating scale-invariant time cells.

Introduction

Behavioral evidence for a scale-invariant internal representation of time

Numerous behavioral experiments in human and other animals suggest that time is represented in the brain in a scale-invariant fashion. For example, in interval timing experiments the accuracy of reproducing a fixed time interval decays with the duration of the interval. More specifically, the variability of the reproduced interval is proportional to the duration of the interval (Rakitin et al., 1998; Ivry & Hazeltine, 1995). The distributions of the response to different intervals are scale-invariant in that they overlap when rescaled by the duration of the interval, a phenomenon termed the scalar property (Gibbon, 1977).

Scale-invariance is also often observed in the associative learning rate in animal conditioning experiments. For instance, it has been shown that the number of trials needed for animals to develop a conditioned response increases when the reinforcement latency is

increased and decreases when the intertrial interval is increased (Gallistel & Gibbon, 2000). Moreover, as long as the ratio between the intertrial interval and the reinforcement latency is fixed, the number of trials needed to develop a conditioned response is fixed, again indicating scale-invariance in the animal's timing behavior.

Results from memory experiments also point to a scale-invariant representation of time. The classic power-law of forgetting (Wixted, 2004) indicates that a single mechanism may underlie both short and long term forgetting. In free recall, subjects are given a list of words and are asked to recall them in any order. The recency effect refers to the phenomenon that words from the end of a list are more easily recalled. This effect has been observed over a wide range of timescales, from fractions of seconds (Murdock & Okada, 1970) to several minutes (Glenberg et al., 1980; Howard, Youker, & Venkatadass, 2008), indicating that a single memory mechanism with a scale-invariant representation of time may serve under different timescales.

Time cells in the brain

Recent neurophysiological recordings in behaving animals show spiking activity at specific temporal intervals by individual neurons, referred to as *time cells*. These experimental data provide a possible neural substrate for the scale-invariant behavior mentioned above (Howard, Shankar, Aue, & Criss, 2015). Time cells fire at different intervals during the delay period when an animal is performing delayed match to sample (MacDonald, Lepage, Eden, & Eichenbaum, 2011), delayed match to category (Tiganj, Cromer, Roy, Miller, & Howard, 2017), spatial alternation (Salz et al., 2016), or temporal discrimination tasks (Tiganj, Kim, Jung, & Howard, in press). Time cells have been found in various parts of the brain including the hippocampus (MacDonald et al., 2011; Salz et al., 2016), PFC (Jin, Fujii, & Graybiel, 2009; Tiganj et al., in press; Bolkan et al., 2017) and striatum (Adler et al., 2012; Mello, Soares, & Paton, 2015; Akhlaghpour et al., 2016). The firing fields of time cells that fire later in the delay period are wider than the firing fields of time cells that fire earlier in the delay period. Moverover, the number density of time cells goes down with delay. Although there is not yet quantitative evidence that time cells are scale-invariant, these findings are qualitatively consistent with a scale-invariant representation. In this paper we consider the potential mechanisms for constructing a scale-invariant population of time cells.

The difficulty to achieve scale-invariance in chaining models

A natural proposal for a model that generates sequentially activated neurons is to connect neurons sequentially in a one-dimensional chain. Goldman (2009) proposed a feed-

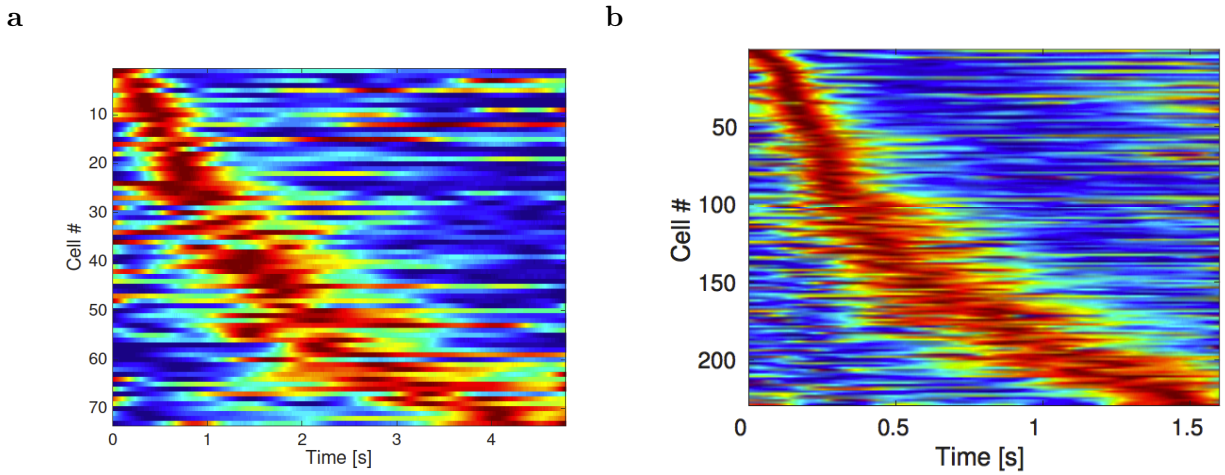

Figure 1. **Sequentially activated neurons in the brain.** Each row on each heatplot displays the normalized firing rate for one time cell. Red corresponds to high firing rate, while blue corresponds to low firing rate. The cells are sorted with respect to the median of the spike time in the delay interval. Two features related to temporal accuracy can be seen from examination of the heatmaps. First, time fields later in the delay are more broad than time fields earlier in the delay. This can be seen as the widening of the central ridge as the peak moves to the right. In addition the peak times of the time cells were not evenly distributed across the delay, with later time periods represented by fewer cells than early time periods. This can be seen in the curvature of the central ridge; a uniform distribution of time fields would manifest as a straight line. **a.** After Tiganj, et al., in press. **b.** After Tiganj, et al., 2017.

forward network model for sustained persistent activity in a network in which a series of neurons modeled by leaky integraters are sequentially connected. In particular, the neurons all have the same decay time constant τ. By solving the dynamical equation it can be shown that their activations are given by the "time basis functions" $r_n(t) = \frac{1}{n!}(\frac{t}{\tau})^n e^{\frac{t}{\tau}}$. However this set of activations is not scale-invariant, as they are not of the same functional form. Figure 2 shows the actual and scaled neuronal activity in the chain. The rescaled neuronal activity becomes more concentrated for the neurons that are activated later.

This property ultimately arises from the Central Limit Theorem. Consider a chain of N neurons where every neuron is modeled by a same synaptic kernel $K(t)$. That is, the activity of every neuron is the convolution of its synaptic kernel with the activity of the previous neuron.

$$g_i(t) = \int_{-\infty}^{t} g_{i-1}(t')K(t-t')dt' \tag{1}$$

Since the functions $K(t)$ and $g_i(t)$ are bounded, we can treat them as probability distribu-

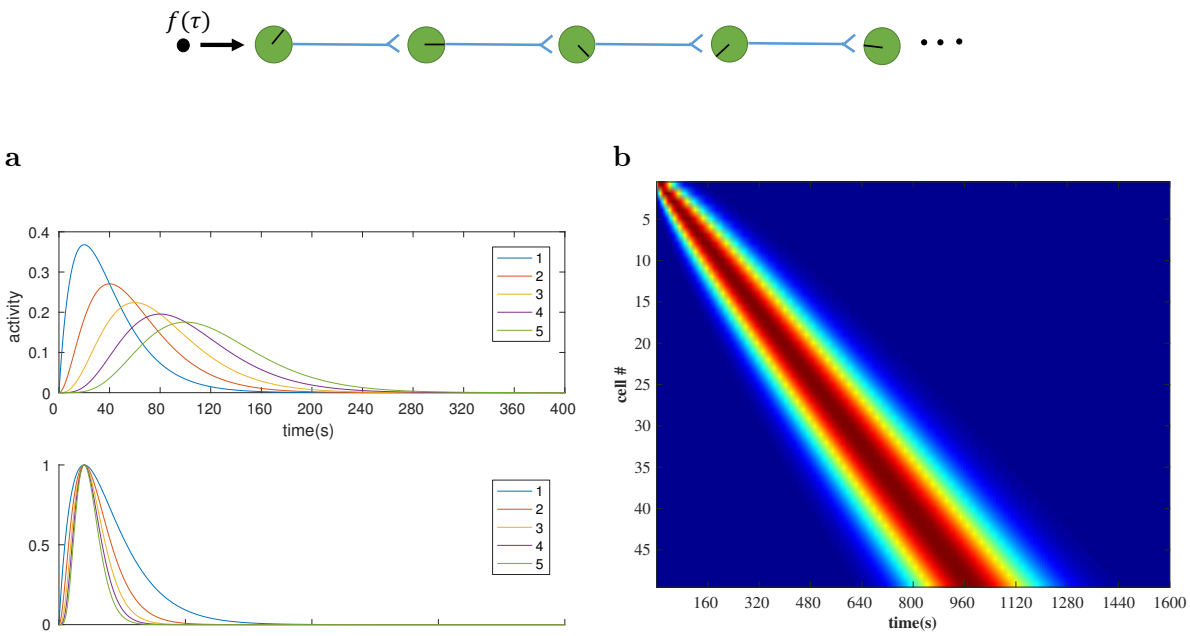

Figure 2. **Simple chaining models produce time cells, but these time cells are not scale-invariant and have properties that differ from experimentally-observed time cells.** Top: A simple chain of units can give rise to sequentially-activated cells. The direction of the 'clock hands' within the neurons indicate the peak firing time of that neuron. **a**. Simulated "time basis functions" constructed from the chaining model described in Goldman (2009). **Top**: 5 successive time basis functions in the chaining model. They represent the neuronal activity for 5 successive nodes along the chain. We set $\tau = 20s$. **Bottom**: The same time basis functions rescaled by the peak time along the x axis and by the maximum activity along the y axis. They deviate from each other systematically. It is clear that the neurons along the chain do not obey scale-invariance. In particular, the activity of neurons that are activated later is more concentrated when rescaled. This can be shown in an asympotic analysis using the Central Limit Theorem (see text). **b**. The heatmap for the activity of 50 neurons in the chaining model. The number of neurons coding later time is the same as the number coding for earlier times. This indicates that these neurons do not represent time in a scale-invariant way.

tions up to a scale factor. Then the activity of the ith neuron $g_i(t)$ is proportional to the probability distribution of the sum of the random variables described by $K(t)$ and $g_{i-1}(t)$. Assuming the kernel K has mean and variance m and σ, then by the Central Limit Theorem, for large i, $g_i(t)$ would have a Gaussian shape with mean im and variance $\sqrt{i}m$. The coefficient of variation (CV) would be smaller for larger i. Therefore when rescaled, the neuronal activity for the neurons that get activated later will be more concentrated. This is indeed what is observed in Figure 2.

Indeed we see that a single time scale, whether in the form of a single time constant for the leaky integrators or a single form of synaptic kernel, does not produce a scale-invariant activation in a chaining model. In this paper we are going to present a neural circuit that instead uses a parallel distribution of neurons with different time constants (Shankar & Howard, 2012) to generate scale-invariant time cells. This gives flexibility to the choice of time constants, and we will therefore choose a series of geometrically spaced time constants to ensure scale-invariance.

Methods

A mathematical approach for constructing a scale-invariant history

The neural circuit presented in this paper is built upon a mathematical framework that has been proposed to construct a representation of the recent past in a distributed, scale-invariant way (Shankar & Howard, 2012, 2013). This mathematical model has two layers of nodes. Nodes in the first layer integrate the stimuli with an exponential kernel, equivalent to performing a Laplace transform on the stimuli. The activity of the nodes in the second layer is obtained by inverting the Laplace transform using the Post approximation. After presenting a delta function as input to the first layer, the activity of units in the second layer resembles the firing rates of scale-invariant time cells. The model can be implemented as a two layer feedfoward neural network where the weights can be explicitly computed as a function of the time constants of the nodes in the first layer. Here we give a brief overview of the mathematical model and emphasize the connection to our neural circuit that will be introduced in section .

Step1: We represent the stimulus that we are interested in as a scalar function over time $f(t)$. This stimulus is fed in parallel into a series of N leaky integrators $F(t, s_i)$ with a spectrum of time constants given by $\tau_i = \frac{1}{s_i}, i = 1, 2, ...N$.

$$\frac{dF(\tau, s_i)}{dt} = -s_i F(t, s_i) + f(t), \qquad i = 1, 2, ...N \tag{2}$$

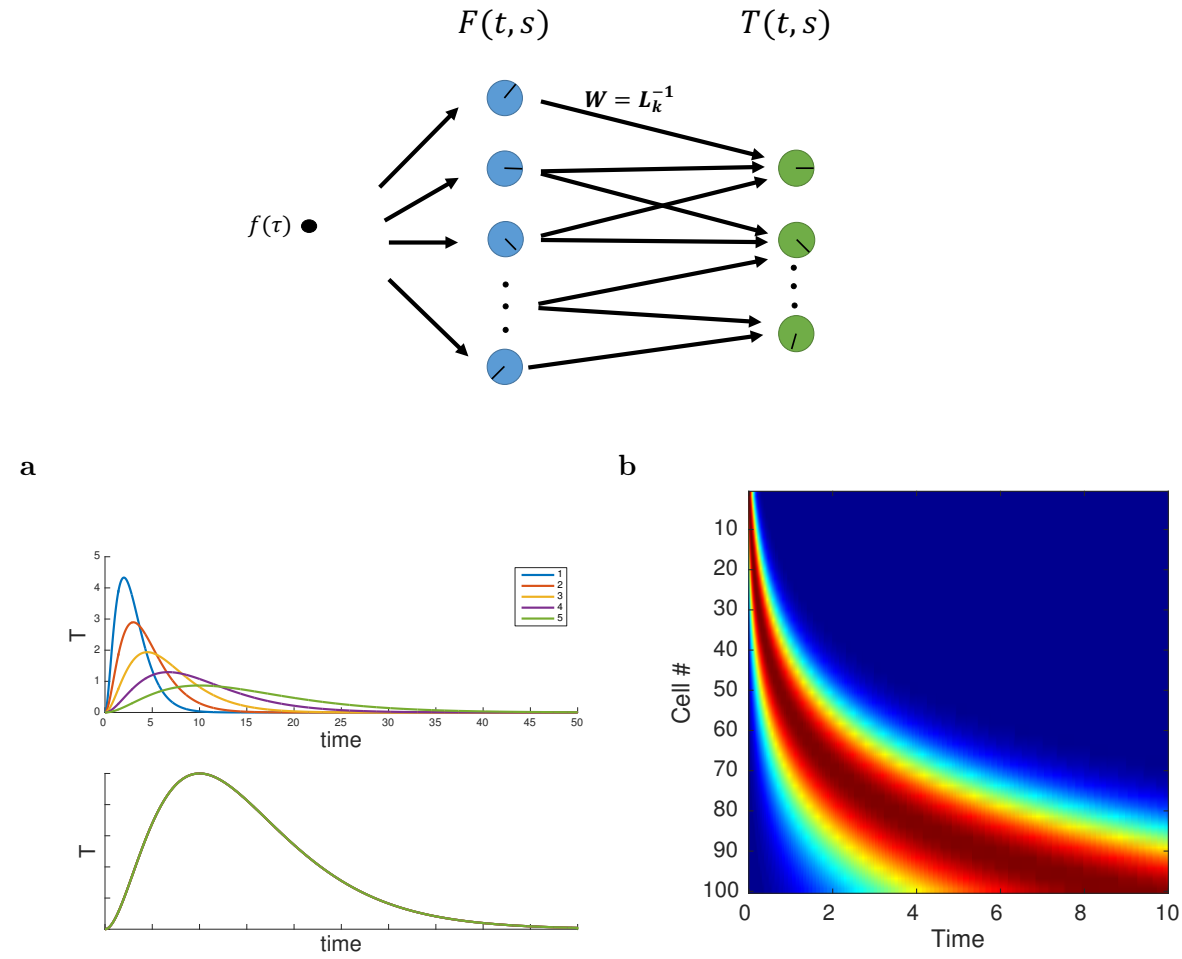

Figure 3. **Illustration of the scale-invariant mathematical model for sequentially-activated time cells.** Top: Rather than a simple chain, in this formulation, an input is provided in parallel to a set of leaky integrators, F. These units provide a feedforward input to another set of units T that function like time cells .The direction of the 'clock hands' within the neurons indicate the time constant of that neuron (peak time for sequentially-activated cells and decay time constant for leaky integrators) **a.** The activation of T nodes after a delta function input in the mathematical model is scale-invariant. **Left:** The activation of 5 T nodes with different time constants $\overset{*}{\tau}$ (Equation 7). $k = 2$ is chosen in the inverse Laplace transform. **Right:** The same functions rescaled by $\overset{*}{\tau}$ along the x axis and by the maximum activation along y axis as in Figure 2. Unlike the chaining model, the five lines exactly overlap each other, showing the scale-invariant property. **b.** Heatmap from the mathematical model. The time at which a time cell activates is ultimately controlled by the time constant of the integrators that provide input to it. Choosing the time constants of the leaky integrators controls the number density of time cells.

Here $F(t, s_i)$ is the activity of the node labeled by s_i. We can observe from Equation 2 that they are just the Laplace transform of the original stimuli with Laplace index s_i.

$$F(t, s_i) = \int_{-\infty}^{t} f(t')e^{-s_i(t-t')}dt' \tag{3}$$

More specifically if we take the stimulus to be a delta function $f(t) = \delta(0)$, the neuron represented by the F node will simply have an exponentially decay firing rate with a decay time constant of $\frac{1}{s_i}$

$$F(t, s_i) \propto e^{-s_i t} \tag{4}$$

Therefore, in this simulation we will assume a stimulus that occurs only at $t = 0$ and model the F nodes as a series of persistent spiking neurons with exponentially decaying firing rates.

Step2: The activity of the F nodes is transformed by a second layer of T nodes. The T nodes are in one-to-one correspondence with the F nodes. At each moment the activity of the F node labeled by s is transformed in the following way:

$$T(t, s) = \frac{(-1)^k}{k!}\ s^{k+1}\ \frac{d^k F(t, s)}{ds^k} \tag{5}$$

Note that in reality we have a discretized spectrum of time constants and we need to discretize the derivative with respect to s as well. We will later show that this discretization offers the possibility of implementing this framework into a feed-forward neural network. But for the purpose of illustrating the mathematical framework, we just assume s to be a continuous label for now.

We introduce a new timescale $\overset{*}{\tau} = \frac{k}{s}$ which we will use later to represent the peak firing time of the time cell.[1] The above transformation is an inverse Laplace transform in the sense that

$$T(t, \overset{*}{\tau}) \approx f(t - \overset{*}{\tau}) \tag{6}$$

where $f(t)$ is the stimulus function in the time leading up to the present (which is defined here as time zero). This approximation becomes exact when $k \to \infty$ (Post, 1930). Thus we can see that the set of functions $T(t, \overset{*}{\tau})$ constitutes a faithful representation of the original stimuli delayed by $\overset{*}{\tau}$.

More specifically, if we adopt the previous setup that stimuli is represented by a delta function and the F nodes are exponentially decaying function, then the T nodes' activity will be

$$T(\tau, s) = \frac{s^{k+1}}{k!}\tau^k e^{-st} = C_k \frac{1}{\overset{*}{\tau}} \left(\frac{t}{\overset{*}{\tau}}\right)^k e^{-k\frac{t}{\overset{*}{\tau}}} \tag{7}$$

[1] This differs from the notation in previous papers by a sign in order to represent a timescale

where C_k is some constant described only in terms of k and we have substituted $\overset{*}{\tau} = \frac{k}{s}$ in the last step.

This function has properties that resemble the firing rate of a time cell with a peak firing rate at $t = \overset{*}{\tau}$, and we will identify them as time cells in our neural circuit. Moreover, the function is only a function of $\frac{t}{\overset{*}{\tau}}$ up to a constant. Thus if we rescale the x axis according to $\overset{*}{\tau}$, and the y axis by the maximum activity, the firing activity of all the cells will coincide, as shown in Figure 3a. In this sense the T node activity is scale-invariant.

This mathematical framework produces a set of functions that resembles the firing rates time cells. Moreover this mechanism gives rise to time cells that are scale-invariant, which would be a desirable property for the brain to possess. However, it is not clear whether it is possible for neural circuits in the brain to actually implement this hypothesized mechanism. We will demonstrate that this is indeed neurally realistic by constructing a biologically detailed neural circuit that utilizes a biophysical model of exponentially decaying persistent firing neuron (Tiganj, Hasselmo, & Howard, 2015) to perform the computation of this mathematical model, thereby generating a set of scale-invariant time cells.

The weight matrix for inverse Laplace transform

The inverse Laplace transform as described in Equation 5 in the introduction will be implemented as a neural network. By Equation 5, the connection weights should depend on the discretized kth derivative with respect to s. To write derivatives in matrix form, imagine there are three successive F nodes, with labels s_{-1}, s_0 and s_1. Note that the first derivative of a function with respect to s_0 can be approximated as a weighted average of the slope of the line connecting the successive points on the curve.

$$\frac{dF(s_0)}{ds} \approx \frac{F(s_1) - F(s_0)}{s_1 - s_0}\left(\frac{s_0 - s_{-1}}{s_1 - s_{-1}}\right) + \frac{F(s_0) - F(s_{-1})}{s_0 - s_{-1}}\left(\frac{s_1 - s_0}{s_1 - s_{-1}}\right) \tag{8}$$

The factors in the brackets account for the fact that the accuracy of the slope further away from the point s_0 is a less accurate estimate of the derivative.[2]

The derivative as expressed in Equation 8 is a linear combination of $F(s_1)$, $F(s_0)$ and $F(s_{-1})$ with coefficients determined by s_1,s_0 and s_{-1}. Therefore if we represent the function $F(s)$ as a vector, where each entry is the value of the function at a specific value of s, or in other words, we discretize the function onto an one-dimensional grid

$$F(s) \to \mathbf{F} \approx [F(s_1), F(s_2), ...F(s_N)]^T \tag{9}$$

[2]This approximation works when the second derivative $\frac{d^2 f(s)}{ds^2}$ does not change sign along the interval $[s_{-1}, s_1]$. This is always the case for exponentially decaying t node activity $t(\tau, s) = e^{-s\tau}$.

we can write the first derivative as a matrix,

$$\frac{d\mathbf{F}}{ds} \approx \mathbf{DF}, \tag{10}$$

where the matrix $\mathbf{D}$ is given by

$$\mathbf{D}_{i,i-1} = -\frac{s_1 - s_0}{(s_0 - s_{-1})(s_1 - s_{-1})} \tag{11}$$

$$\mathbf{D}_{i,i} = \frac{s_1 - s_0}{(s_0 - s_{-1})(s_1 - s_{-1})} - \frac{s_0 - s_{-1}}{(s_1 - s_0)(s_1 - s_{-1})} \tag{12}$$

$$\mathbf{D}_{i,i+1} = \frac{s_0 - s_{-1}}{(s_1 - s_0)(s_1 - s_{-1})} \tag{13}$$

for $i = 1, 2, \ldots, N$ and all the other elements are 0. The kth derivative can be obtained by simply multiplying k of these matrices.

$$\frac{d^k\mathbf{F}}{ds^k} \approx \mathbf{D}^k\mathbf{F} \tag{14}$$

After we have the matrix representation of the kth derivative, the activity for a given T node $T(t, s)$ can be approximated by a linear combination of the F node activities $F(t, s)$.

$$\mathbf{T}(t) \approx \frac{(-1)^k}{k!}\mathbf{s^{k+1}} \odot \mathbf{D}^k\mathbf{F}(t) \equiv \mathbf{L}_k^{-1}\mathbf{F}(t) \tag{15}$$

where $\odot$ represents element-wise multiplication, and $\mathbf{s^{k+1}} = [s_1^{k+1}, s_2^{k+1}, ...s_N^{k+1}]^T$. Thus the inverse Laplace transform is readily implemented in a neural network via a weight matrix $\mathbf{L}_k^{-1}$. In our simulation we choose $k = 2$, so for a given T node labeled by s_0 its activity at any given time t will depend on its five nearest neighboring F nodes, $F(t, s_{-2})$,$F(t, s_{-1})$,$F(t, s_0)$,$F(t, s_1)$ and $F(t, s_2)$. In this simulation, we have 9 presynaptic F nodes labeled by s_1 to s_9. According to above they will generate 5 postsynaptic T nodes.

A biophysical model of exponentially decaying persistent firing neurons

As mentioned above, if we model the input stimuli as a delta function, the F nodes will behave as persistent spiking neurons with exponentially decaying firing rates. However if we want to have time cells that peak at as long as tens of seconds after the stimuli is presented, we need to have persistent firing neurons that have a decay constant comparable to that timescale, since they are related by $\overset{*}{\tau} = \frac{k}{s}$. It is non-trivial to identify a biophysical mechanism that can result in persistent spiking that lasts over that period of time. Tiganj et al. (2015) developed a computational model of single neurons that uses a calcium-activated nonspecific (CAN) cationic current to achieve decay time constants up to several tens of seconds under realistic choice of parameters. Here we utilize that same model as the neural realization of the F nodes.

The dynamics of the model is summarized as follows:

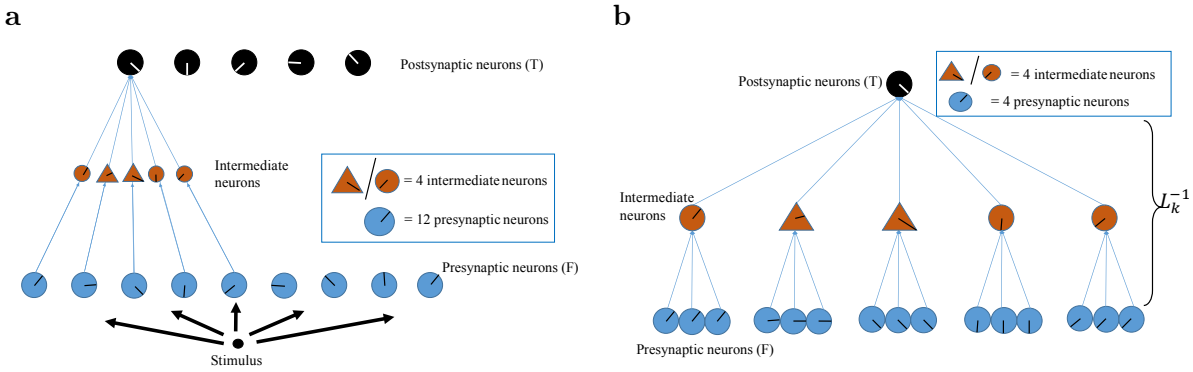

Figure 4. **Schematic of the architecture of the biological network. a.** Only a subset of the intermediate neurons are drawn. Blue circle: presynaptic neurons. Orange circle: excitatory intermediate neurons. Orange triangle: inhibitory intermediate neurons. Black circle: postsynaptic neurons. The direction of the 'clock hands' within the neurons indicate the time constant of that neuron. In the actual simulation, 9 groups of 12 persistent spiking neurons connect to 5 postsynaptic neurons (later identified as time cells) via weights generated by a matrix representation of the inverse Laplace transform $\mathbf{L}_k^{-1}$. In order to satisfy Dale's Law, an excitatory/inhibitory intermediate neuron is placed on each positive/negative connection. **b.** The upstream neurons of one time cell. Every 3 presynaptic cells with the same decay time constant project to one intermediate cell. Twenty intermediate neurons with different time constants and different PSP amplitudes project to one time cell, neurally implementing the weight matrix $\mathbf{L}_k^{-1}$.

1. During the interspike interval, the membrane potential $v_m(t)$ is modeled to be only affected by the CAN current

$$C_m \frac{dv_m(t)}{dt} = -i_{\text{CAN}}(t). \tag{16}$$

where C_m is the membrane capacitance and i_{CAN} is the CAN current.

2. The CAN current is given by

$$i_{\text{CAN}}(t) = \bar{g}_{\text{CAN}}\ m\,[v_m\,(t) - E_{\text{CAN}}] \tag{17}$$

Here $\bar{g}_{\text{CAN}}$ is the maximal value of the ion conductance measured in $\frac{mho}{cm^2}$, E_{CAN} is the reversal potential of the CAN current ion channels and m is a dimensionless quantity between 0 and 1 that is associated with the activation of the CAN current ion channels.

3. Following previous computational work (Traub, Wong, Miles, & Michelson, 1991; Fransén, Alonso, & Hasselmo, 2002), we let the activation parameter for the ion channel m change from moment to moment according to

$$\frac{dm}{dt} = a\ \text{Ca}(t)(1-m) - b\,m \tag{18}$$

where a and b are free parameters. Following Fransén et al. (2002), we choose them to be 0.02 and 1, respectively, in this simulation.

4. The dynamics of the calcium is given by an exponential decay during interspike interval with a decay time constant τ_p.

$$\frac{d\mathrm{Ca}(t)}{dt} = \frac{-\mathrm{Ca}(t)}{\tau_p} \tag{19}$$

where τ_p is the decay time constant, as well as a fixed amount influx of calcium whenever the cell fires an action potential.

$$\mathrm{Ca}(t) \to \mathrm{Ca}(t) + k_{\mathrm{Ca}} \tag{20}$$

Tiganj et al. (2015) showed both analytically and numerically that under the appropriate assumptions the firing rate will be approximately exponentially decaying with a decay time constant of

$$\frac{1}{\tau} = \frac{1}{\tau_p} + \frac{\bar{g}_{\mathrm{CAN}}\ k_{Ca}\ \gamma}{Q} \tag{21}$$

where $\gamma = a\,(\bar{v}_m - E_{\mathrm{CAN}})$, $\bar{v}_m$ is the average membrane potential during a spike and Q is the total charge influx during a spike. This expression requires that the change of m is much faster than the change of calcium i.e. $\frac{1}{a\mathrm{Ca}(t)+b} \ll \tau_p$ and the interspike interval is much less than the decay time constant of the calcium concentration. In the simulation we choose the parameters to satisfy the two conditions above, so that the firing rates are well approximated by exponential decaying functions.

The basic set-up of the model

The neural circuit that we are going to present will implement the inverse Laplace transform $\mathbf{L}_k^{-1}$ in the mathematical model using biophysically realistic neurons. In this simulation, we choose $k = 2$. The neural circuit consists of 108 presynaptic neurons modeling the F nodes in the mathematical model. They are the CAN current driven, persistent firing neurons described above. They span 9 different time constants with 12 neurons for each time constant. To model the experimental finding of logarithmically-compressed timeline, the time constants are chosen to be 10.85 s,16.91 s, 27.21 s, 45.83 s, 83.49 s logarithmically spaced between 2 s and 83 s by adjusting calcium conductance g_{CAN} and initial calcium concentration in the CAN driven persistent firing neuron model above according to Table 2. All the model parameters are summarized in Table 2

The 9 groups of presynaptic neurons are connected to 5 postsynaptic neurons (time cells) via connection matrix $\mathbf{L}_k^{-1}$ with $k = 2$. However, a direct connection would violate

Dale's Law as there can be both positive and negative weights in the same row of the weight matrix $\mathbf{L}_k^{-1}$, which requires some presynaptic neurons to have both excitatory and inhibitory connections. To ensure adherence to Dale's law we place an intermediate neuron on every connection. The intermediate neurons are inhibitory or excitatory depending on the sign of the connection weight that they implement, as shown in Figure 4.

To keep the firing rates of the intermediate neurons in a reasonable regime, the PSPs coming from 3 presynaptic neurons from the same group are used as the input to one intermediate neuron, which we model as leaky integrate and fire neurons. The time evolution of the intermediate neurons is

$$V_{\text{int}}(t+\triangle t) = V_{\text{int}}(t) + \frac{\triangle t}{\tau_{\text{int}}}\left(-\left[V_{\text{int}}(t) - E_{\text{int}}\right] + \sum_{i=1}^{3} \text{PSP}_{\text{pre},i}(t) + 0.5\mathscr{U}(0,1)\right) \tag{22}$$

where E_{int} is the resting potential for the intermediate neurons, τ_{int} is the membrane time constant, $\text{PSP}_{\text{pre},i}$ is the PSP coming from pre synaptic neuron i and a noise term $\mathscr{U}(0,1)$ represents a random number drawn uniformly from (0,1). We add a noisy background current of amplitude 0.5 so that the intermediate neurons are in their linear regime, an essential point to ensure scale-invariance. We will discuss it further in the discussion section.

The PSPs generated by the intermediate neurons with 5 different time constants are summed up and provided as the input to the postsynaptic neurons, as in Figure 4b. The weight matrix $\mathbf{L}_k^{-1}$ is neurally implemented by adjusting the amplitude of the PSPs for each intermediate neuron according to Table 1. This will ensure each intermediate neuron contributes to the postsynaptic neuron in a proportion according to the weight matrix $\mathbf{L}_k^{-1}$. We also rescale the individual PSPs so that the inputs to the different postsynaptic neurons have the same maximum. This ensures that the postsynaptic neurons are all in their linear regime. This could be due to homeostatic synaptic scaling in which the activity of neurons regulates the magnitude of synaptic inputs. (Turrigiano, Leslie, Desai, Rutherford, & Nelson, 1998)

The postsynaptic neurons are also leaky integrate and fire neurons with the same parameters as the intermediate neurons.

$$V_{\text{post}}(t+\triangle t) = V_{\text{post}}(t) + \frac{\triangle t}{\tau_{\text{post}}}\left(-\left[V_{\text{post}}\,(t) - E_{\text{post}}\right] + \sum_{i=1}^{5}\sum_{j=1}^{4} \text{PSP}_{\text{int},i,j}(t)\right) \tag{23}$$

where i indexes different time constants and j indexes the different intermediate neurons with the same time constant. We use alpha functions for modeling the synaptic potentials. We use MATLAB 2016a to run the simulation with a time step of 0.1 ms.

PSP amplitude(μV)	j = 1	2	3	4	5	6	7	8	9
i = 1	15.4	45.2	-174.8	-587.7	193.5				
2		10.5	40.1	-197.9	-342.1	129.4			
3			6.7	19.1	-90.1	-186.5	66.4		
4				4.4	12.7	-67.5	-135.5	50.5	
5					1.6	5.3	-17.2	-66.1	20.9

Table 1: The PSP amplitude for each intermediate neuron labeled by its upstream presynaptic neuron j (j ranges from 1 to 9) and downstream postsynaptic neuron i (i ranges from 1 to 5). They are computed from Equation 15 by substituting the time constants from Table 2.

Results

The primary result of this paper is that the simulated postsynaptic neurons fired sequentially in response to a delta function input like time cells and that the sequential firing was approximately scale-invariant. Before describing that result, we first describe the activity profile of each of the intermediate layers in turn.

Presynaptic neurons showed exponential decay with a range of time constants

The presynaptic neurons as shown in the bottom layer of Figure 4 are CAN current driven, persistent firing neurons that have exponentially decaying firing rates. These cells are driven by the input to the network. The decay time constants are logarithmically spaced between 2.04 s and 83.49 s. This is achieved by adjusting the calcium conductance g_{CAN} and initial calcium concentration according to Table 2. We fitted a series of exponentials in dotted line to confirm the firing rates are indeed exponentially decaying. This is in accordance with the activity of the F nodes in the mathematical model.

There are 9 groups of presynaptic neurons in total, each group has the same time constant. Within each group there are 12 presynaptic neurons with the same parameters. For every 3 of them, their PSPs are summed up and sent as input to one intermediate neuron, as shown in Equation 22 and Figure 4b.

Intermediate cells also decayed exponentially

The intermediate cells shown in the middle layer of Figure 4 are leaky integrate and fire neurons. Their parameters are shown in Table 2. Driven by upstream neurons with exponentially decaying firing rates, they also display firing rates that decay exponentially,

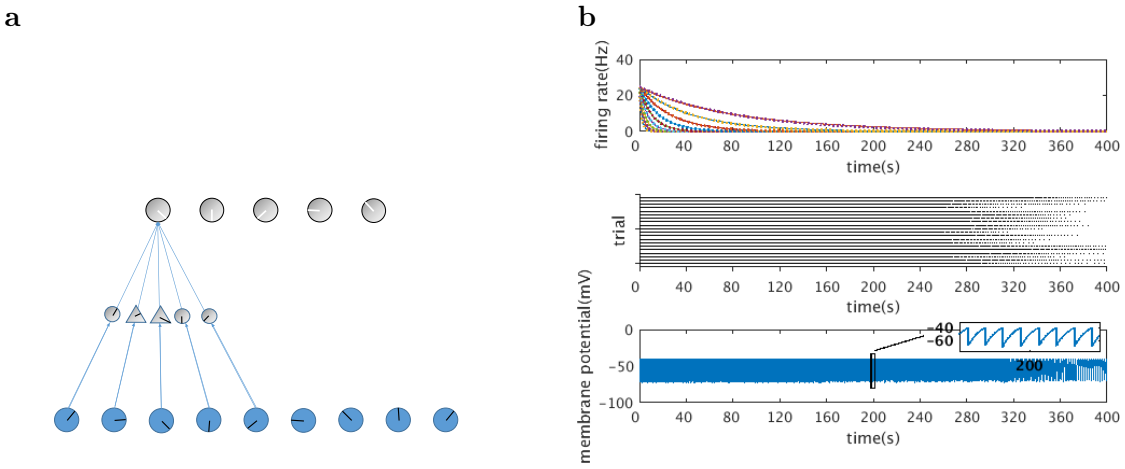

Figure 5. **The input layer of neurons encoding the Laplace transform decays exponentially. a.** The bottom layer is composed of presynaptic neurons which we model as exponentially decaying persistent spiking neurons due to the CAN current. These cells are driven by the network input. **b.** Top: Firing rates for the persistent firing neurons. Nine example neurons with time constants logarithmically spaced between 2.04 s and 83.49 s are shown. Middle: Rasterplot for an example neuron with a time constant of 83.49 s. Bottom: Membrane potential for the same example neuron. All firing rates are averaged over 100 trials.

at least initially. At later time points they maintain a background firing rate of around 10 Hz due to the background current as described in Equation 22. This ensures that the intermediate neurons are always in the linear regime, which is crucial for exact scale-invariance of the computation performed by this neural circuit (Figure 7).

The PSPs of the intermediate neurons contribute differently to the postsynaptic neurons due to the different amplitude of their individual PSPs as shown in Table 1. The PSPs of intermediate neurons with 5 different time constants provide input to one postsynaptic neuron, as shown in Figure 4b. Since each intermediate neuron is only involved in one connection, Dale's Law is satisfied by simply choosing the intermediate neuron to be excitatory if it corresponds to a positive weight, and vice versa. For this particular simulation, the excitatory neurons have NMDA receptors with a time constant of 45 ms (Otis & Mody, 1992) and the inhibitory neurons have $GABA_A$ receptors with a time constant of 15 ms. (Perouansky & Yaari, 1993)

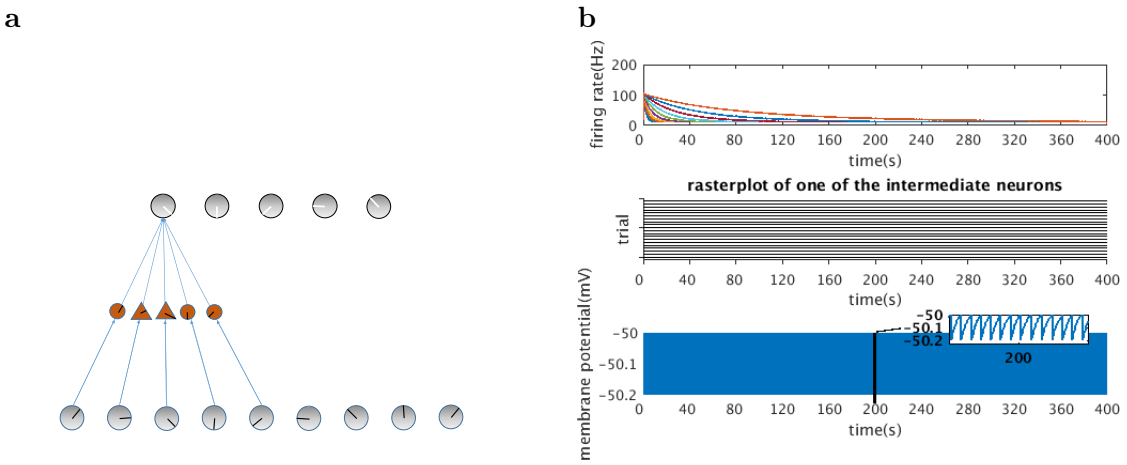

Figure 6. **Intermediate neurons decay exponentially to a constant background firing rate. a.** The middle layer is composed of intermediate neurons which we model as leaky integrate and fire neurons. They are driven directly by the downstream persistent spiking neurons. They serve the role of exciting and inhibiting the neural activity from the bottom layer to the top layer in order to complete the computation of the inverse Laplace transform. **b.** Firing rates for 9 intermediate neurons with different decay constants. The rasterplot and membrane potential are hard to discern due to background firing. All firing rates are averaged over 100 trials.

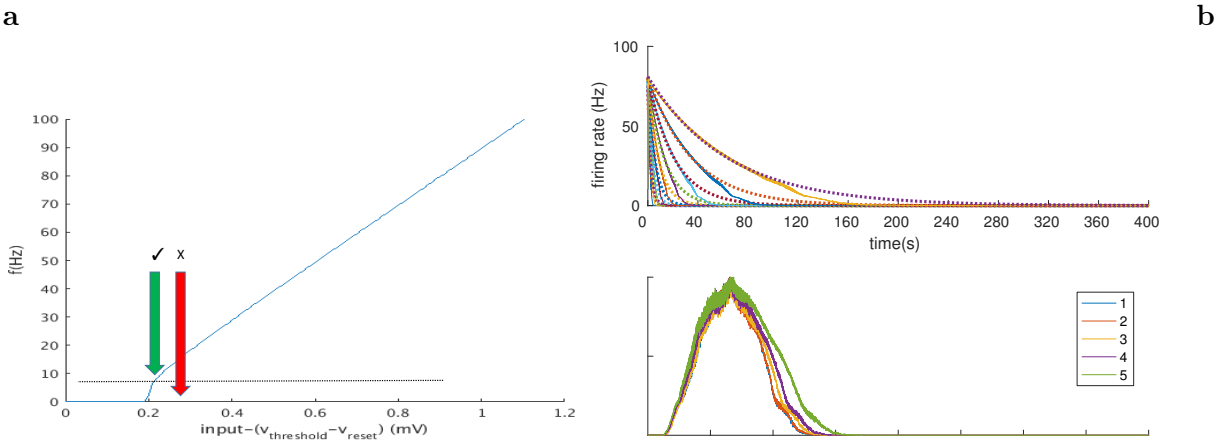

Figure 7. **a.** The f-I curve for an intermediate neuron is composed of two linear regimes. 'kink' separating the regimes at around 10 Hz is indicated by the horizontal dotted line. If the firing rate crossed this kink, it would result in violations of scale-invariance in the post-synaptic cells. The background input in the simulation keeps the firing rate in the linear regime enabling scale-invariance in the sequentially-activated post-synaptic cells. **b.** The rescaled post-synaptic firing rates with the same parameters as in the main simulation, but without the background inputs.

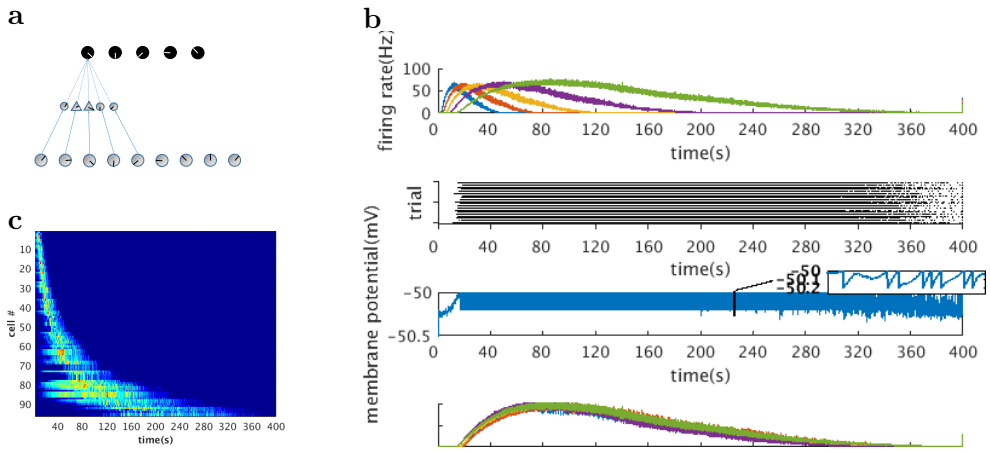

Figure 8. **This method produces scale-invariant time cells that resemble neural data. a.** The top layer consists of 5 leaky integrate and fire neurons which we identify as time cells. **b.** From top to bottom: Postsynaptic firing rates for the 5 time cells generated by this network. Rasterplot for the neuron with the widest receptive field; Membrane potential for the same neuron; Rescaled version of the firing rates. It is clear that the firing rates coincide with each other when rescaled, showing that the firing rates for the time cells are indeed scale-invariant. Firing rates are averaged over 100 trials. **c.** Heatmap generated from 100 simulated time cells. Compare to Figure 1 and 2b.

Post-synaptic neurons fired sequentially and were approximately scale-invariant

The post-synaptic cells shown in the top layer of Figure 4 are also modeled as leaky integrate and fire neurons. When driven by the PSPs from the intermediate neurons, their firing rates resemble the mathematical expression of Equation 7. As shown in Figure 8 their peak firing times scale with the width of their firing fields. When rescaled according to peak firing time, their firing rates overlap with each other. This indicates that the postsynaptic neurons fire sequentially and have a firing rate profile that is time-scale invariant.

Discussion

We proposed a neural circuit that performs the computation of the inverse Laplace transform to produce a series of sequentially firing cells with peak firing times ranging from a few seconds to almost 100 seconds. Critically, their firing rates are scale-invariant. This provides a possible neural substrate for the scalar timing behavior observed across a wide range of timescales in behavioral tasks, and also approximates the neurophysiological recordings of sequentially activated cells that have been observed across a wide range of regions of the cortex including the hippocampus(MacDonald et al., 2011; Salz et al., 2016), PFC (Tiganj et al., in press) and striatum (Adler et al., 2012; Mello et al., 2015).

We also show the biological constraints on the neural circuit that can cause deviation from scale-invariance. We demonstrate that linearity of the neuronal input output function is required to ensure scale-invariance. This required some background firing for the intermediate neurons. It would also allow background firing for the presynaptic neurons. A constant shift in $F(t, s)$ (with noise) would not affect the derivative in the inverse Laplace transform.

Additional biological features of this model are the use of decaying persistent spiking activity, which resembles the persistent firing properties observed in intracellular recordings from slice preparations of the entorhinal cortex (Klink & Alonso, 1997; Tahvildari, Fransén, Alonso, & Hasselmo, 2007; Jochems, Reboreda, Hasselmo, & Yoshida, 2013; Egorov, Hamam, Fransén, Hasselmo, & Alonso, 2002). Mechanisms of decaying persistent firing has also been observed in other structures such as hippocampus (Knauer, Jochems, Valero-Aracama, & Yoshida, 2013) and prefrontal cortex (HajDahmane & Andrade, 1996).

This model also has implications for the patterns of synaptic connectivity between different populations of neurons in the cortical regions involved in the generation of time cells. In particular, it suggests a specific pattern of connectivity between neurons with different time constants of decaying persistent spiking, both excitatory and inhibitory, with time cells. In this simulation we chose a specific series of time constants and $k = 2$ in the inverse Laplace transform, and the connectivity pattern is shown in Table 1. For any choice of time constants and k value, the general form of connectivity can be derived from the matrix $\mathbf{L}_k^{-1}$ in Equation 15. Current techniques for determining connectivity do not allow analysis of connectivity at the level of detail necessary to test this experimentally, but we have endeavored to keep this connectivity within biologically realistic constraints by retaining Dale's law with different populations of neurons mediating excitatory and inhibitory synaptic potentials. Future experimental data on large scale population dynamics might allow analysis of the correlation of different neurons to determine their potential role in computing the inverse Laplace transform.

There are other neural circuit models that produce sequentially activated neurons, but to our knowledge, our model is the first one that has the additional feature of scale-invariant neuronal activity. It still remains to be seen whether the firing activity of the time cells in neurophysiological data is scale-invariant. The currently available recordings (e.g. (MacDonald et al., 2011; Kraus, Robinson, White, Eichenbaum, & Hasselmo, 2013)) do not give a quantitatively conclusive answer due to low temporal resolution and low sample size. Future neurophysiological recordings involving large scale high temporal resolution could potentially confirm the exact firing pattern of these time cells and shed light on the

mechanisms that generate their firing properties.

Acknowledgments

The authors gratefully acknowledge support from MURI N00014-16-1-2832 and NIBIB R01EB022864.

References

Adler, A., Katabi, S., Finkes, I., Israel, Z., Prut, Y., & Bergman, H. (2012). Temporal convergence of dynamic cell assemblies in the striato-pallidal network. *Journal of Neuroscience*, *32*(7), 2473-84. doi: 10.1523/JNEUROSCI.4830-11.2012

Akhlaghpour, H., Wiskerke, J., Choi, J. Y., Taliaferro, J. P., Au, J., & Witten, I. (2016). Dissociated sequential activity and stimulus encoding in the dorsomedial striatum during spatial working memory. *eLife*, *5*, e19507.

Bolkan, S. S., Stujenske, J. M., Parnaudeau, S., Spellman, T. J., Rauffenbart, C., Abbas, A. I., ... Kellendonk, C. (2017). Thalamic projections sustain prefrontal activity during working memory maintenance. *Nature Neuroscience*.

Egorov, A. V., Hamam, B. N., Fransén, E., Hasselmo, M. E., & Alonso, A. A. (2002). Graded persistent activity in entorhinal cortex neurons. *Nature*, *420*(6912), 173-8.

Fransén, E., Alonso, A. A., & Hasselmo, M. E. (2002). Simulations of the role of the muscarinic-activated calcium-sensitive nonspecific cation current INCM in entorhinal neuronal activity during delayed matching tasks. *Journal of Neuroscience*, *22*(3), 1081-1097.

Gallistel, C. R., & Gibbon, J. (2000). Time, rate, and conditioning. *Psychological Review*, *107*(2), 289-344.

Gibbon, J. (1977). Scalar expectancy theory and Weber's law in animal timing. *Psychological Review*, *84*(3), 279-325.

Glenberg, A. M., Bradley, M. M., Stevenson, J. A., Kraus, T. A., Tkachuk, M. J., & Gretz, A. L. (1980). A two-process account of long-term serial position effects. *Journal of Experimental Psychology: Human Learning and Memory*, *6*, 355-369.

Goldman, M. S. (2009). Memory without feedback in a neural network. *Neuron*, *61*(4), 621–634.

HajDahmane, S., & Andrade, R. (1996). Muscarinic activation of a voltage-dependent cation nonselective current in rat association cortex. *Journal of Neuroscience*, *16*(12), 3848–3861. Retrieved from `http://www.jneurosci.org/content/16/12/3848`

Howard, M. W., Shankar, K. H., Aue, W., & Criss, A. H. (2015). A distributed representation of internal time. *Psychological Review*, *122*(1), 24-53.

Howard, M. W., Youker, T. E., & Venkatadass, V. (2008). The persistence of memory: Contiguity effects across several minutes. *Psychonomic Bulletin & Review*, *15*(PMC2493616), 58-63.

Ivry, R. B., & Hazeltine, R. E. (1995, Feb). Perception and production of temporal intervals across a range of durations: evidence for a common timing mechanism. *J Exp Psychol Hum Percept Perform*, *21*(1), 3-18.

Jin, D. Z., Fujii, N., & Graybiel, A. M. (2009). Neural representation of time in cortico-basal ganglia circuits. *Proceedings of the National Academy of Sciences*, *106*(45), 19156–19161.

Jochems, A., Reboreda, A., Hasselmo, M. E., & Yoshida, M. (2013). Cholinergic receptor activation supports persistent firing in layer iii neurons in the medial entorhinal cortex. *Behavioural Brain Research*, *254*, 108-15. doi: 10.1016/j.bbr.2013.06.027

Klink, R., & Alonso, A. (1997). Muscarinic modulation of the oscillatory and repetitive firing properties of entorhinal cortex layer II neurons. *Journal of Neurophysiology*, *77*(4), 1813-1828.

Knauer, B., Jochems, A., Valero-Aracama, M. J., & Yoshida, M. (2013). Long-lasting intrinsic persistent firing in rat ca1 pyramidal cells: A possible mechanism for active maintenance of memory. *Hippocampus*.

Kraus, B. J., Robinson, R. J., 2nd, White, J. A., Eichenbaum, H., & Hasselmo, M. E. (2013). Hippocampal "time cells": time versus path integration. *Neuron*, *78*(6), 1090-101. doi: 10.1016/j.neuron.2013.04.015

MacDonald, C. J., Lepage, K. Q., Eden, U. T., & Eichenbaum, H. (2011). Hippocampal "time cells" bridge the gap in memory for discontiguous events. *Neuron*, *71*(4), 737-749.

Mello, G. B., Soares, S., & Paton, J. J. (2015). A scalable population code for time in the striatum. *Current Biology*, *25*(9), 1113–1122.

Murdock, B. B., & Okada, R. (1970). Interresponse times in single- trial free recall. *Journal of Verbal Learning and Verbal Behavior*, *86*, 263-267.

Otis, T., & Mody, I. (1992). Modulation of decay kinetics and frequency of gabaa receptor-mediated spontaneous inhibitory postsynaptic currents in hippocampal neurons. *Neuroscience*, *49*(1), 13 - 32. Retrieved from `http://www.sciencedirect.com/science/article/pii/030645229290073B` doi: http://dx.doi.org/10.1016/0306-4522(92)90073-B

Perouansky, M., & Yaari, Y. (1993). Kinetic properties of nmda receptor-mediated synaptic currents in rat hippocampal pyramidal cells versus interneurones. *The Journal of Physiology*, *465*(1), 223–244. Retrieved from `http://dx.doi.org/10.1113/jphysiol.1993.sp019674` doi: 10.1113/jphysiol.1993.sp019674

Post, E. (1930). Generalized differentiation. *Transactions of the American Mathematical Society*, *32*, 723-781.

Rakitin, B. C., Gibbon, J., Penny, T. B., Malapani, C., Hinton, S. C., & Meck, W. H. (1998). Scalar expectancy theory and peak-interval timing in humans. *Journal of Experimental Psychology: Animal Behavior Processes*, *24*, 15-33.

Salz, D. M., Tiganj, Z., Khasnabish, S., Kohley, A., Sheehan, D., Howard, M. W., & Eichenbaum, H. (2016). Time cells in hippocampal area CA3. *Journal of Neuroscience*, *36*, 7476-7484.

Shankar, K. H., & Howard, M. W. (2012). A scale-invariant internal representation of time. *Neural Computation*, *24*(1), 134-193.

Shankar, K. H., & Howard, M. W. (2013). Optimally fuzzy temporal memory. *Journal of Machine Learning Research*, *14*, 3753-3780.

Tahvildari, B., Fransén, E., Alonso, A. A., & Hasselmo, M. E. (2007). Switching between "On" and "Off" states of persistent activity in lateral entorhinal layer III neurons. *Hippocampus*, *17*(4), 257-63.

Tiganj, Z., Cromer, J. A., Roy, J. E., Miller, E. K., & Howard, M. W. (2017). Compressed timeline of recent experience in monkey lpfc. *bioRxiv*, 126219.

Tiganj, Z., Hasselmo, M. E., & Howard, M. W. (2015). A simple biophysically plausible model for long time constants in single neurons. *Hippocampus*, *25*(1), 27-37.

Tiganj, Z., Kim, J., Jung, M. W., & Howard, M. W. (in press). Sequential firing codes for time in rodent mPFC. *Cerebral Cortex*.

Traub, R. D., Wong, R. K., Miles, R., & Michelson, H. (1991). A model of a ca3 hippocampal pyramidal neuron incorporating voltage-clamp data on intrinsic conductances. *Journal of Neurophysiology*, *66*(2), 635–650. Retrieved from `http://jn.physiology.org/content/66/2/635`

Turrigiano, G. G., Leslie, K. R., Desai, N. S., Rutherford, L. C., & Nelson, S. B. (1998, 2). Activity-dependent scaling of quantal amplitude in neocortical neurons. *Nature*, *391*(6670), 892–896. Retrieved from `http:https://doi.org/10.1038/36103` doi: 10.1038/36103

Wixted, J. T. (2004). The psychology and neuroscience of forgetting. *Annu. Rev. Psychol.*, *55*, 235–269.

Variable	Label	Value
	Presynaptic Neurons	
threshold potential	v_t	-40mV
reset potential	v_{reset}	-70mV
reversal potential of CAN current	e_{CAN}	-20mV
capacitance	C_m	10^{-4} μF
calcium decay constant	τ_p	1000ms
dynamical parameter for m	a	0.02
another dynamical parameter for m	b	1
calcium conductance	g_{CAN}	$0.0023, 0.0031, 0.0036, 0.0039, 0.0042, 0.0043, 0.0044, 0.0045, 0.0045 mho/cm^2$
calcium influx every spike	K	0.001 (calcium concentration is defined to be unitless)
initial calcium concentration	$Ca(0)$	0.05/0.0376/0.0322/0.0294/0.0278/0.0268/0.0262/0.0258/0.0255
	Intermediate Neurons	
time constant	τ_i	50ms
threshold potential	$v_{t,i}$	-50mV
reset potential	$v_{reset,i}$	-50.2 mV
	Postsynaptic Neurons	
time constant	τ_{post}	50ms
threshold potential	$v_{t,post}$	-50mV
reset potential	$v_{reset,post}$	-50.2 mV
	Synaptic Potenial (modeled as alpha function)	
time constant for NMDA receptor	$\tau_{alpha,NMDA}$	45ms
time constant for $GABA_A$ receptor	$\tau_{alpha,GABA}$	15ms
duration of a single synaptic potential		300ms

Table 2: List of the parameters of the model